Natural-convection Heat Transfer in Regions of Maximum Fluid Density

R. S. SCHECHTER, University of Texas, Austin, Texas

H. S. ISBIN, University of Minnesota, Minneapolis, Minnesota

One of the important factors affecting the rate of heat transfer by natural convection is the temperature-density relationship of the convecting fluid. The importance of this factor is amplified when the heat is being transferred to a medium which has a maximum density.

This investigation consisted of measuring the heat transfer rates, velocity gradients, and temperature profiles when heat is transferred from a flat vertical plate to water in the region of 4°C. In some experiments the flow in the boundary layer was observed to be downward while at other conditions of plate and fluid temperature a dual motion (both up and down) was noted, thus establishing a basic difference in the heat transfer mechanism and precluding a unified theory. Theoretical consideration is given to each mechanism and a criterion is derived to predict the flow regime which will prevail at fixed conditions of plate and bulk temperatures.

An analogue computer was used to establish theoretical velocity and temperature profiles. The theoretical values agree reasonably well with the measured values; however, the experimental temperature gradients near the wall were not sufficiently accurate to be extrapolated to determine a point heat transfer coefficient.

For the usual conditions governing natural convection, the following equations are used to describe the motion, heat conduction, and continuity conditions (*4*):

$$\rho\left(u\frac{\partial u}{\partial x}+v\frac{\partial u}{\partial y}\right) = g(\rho_\infty-\rho)+\mu\frac{\partial^2 u}{\partial y^2} \quad (1)$$

$$\frac{\partial u}{\partial x}+\frac{\partial v}{\partial y}=0 \quad (2)$$

$$u\frac{\partial T}{\partial x}+v\frac{\partial T}{\partial y}=\alpha\frac{\partial^2 T}{\partial y^2} \quad (3)$$

With boundary conditions

$$\begin{aligned} &t=t_p \quad u=0 \quad v=0 \quad \text{at} \quad y=0 \\ &t=t_\infty \quad u=0 \quad v=0 \quad \text{at} \quad y=\infty \end{aligned} \quad (4)$$

The coordinates for the vertical-plate geometry are given in Figure 1. The boundary-layer thickness is assumed to be small in comparison with the length of the plate and, therefore, the second derivatives with respect to x have been neglected. Further, Equations (1), (2), (3), and (4) are written with incompressibility of the fluid, steady state, two-dimensional flow, a constant surface temperature, and a constant density throughout the fluid assumed except in the evaluation of the quantity $(\rho_\infty - \rho)$.

This quantity, which appears in Equation (1), represents the driving force that produces the convection currents. This term is normally (i.e., for cases in which the density of the convecting fluid decreases uniformly with increasing values of the temperature) positive for a heating process and negative for a cooling process. A positive driving force indicates that the force is in the positive x direction.

The magnitudes and directions of the driving forces acting upon a convecting medium are a function of the temperature gradients within the boundary layer and the density-temperature relationship. In that the density of water is a maximum at 4°C., convective heat transfer to water in the region of 4°C. can produce a situation in which both positive and negative forces are acting on the fluid. An example is the forces which exist when a plate that is maintained at 12°C. is immersed in a water bath cooled to 1°C. The driving force is positive at those points within the boundary layer at which the water temperature is greater than 7.04°C., since the quantity $(\rho - \rho_\infty)$ is positive. The term $(\rho - \rho_\infty)$ becomes negative when the water temperature is less than 7.04°C. and is zero at 7.04°C. Owing to the existence of both positive and negative driving forces, fluid motion should occur in both the upward and downward directions simultaneously.

Dumore, Prins, and Merk (*1*) studied the heat transfer characteristics of ice spheres immersed in a water bath. They demonstrated experimentally that the heat transfer coefficient tended toward a minimum value at a bath temperature of 4.8°C. These experimenters suggested that the convective motion within the boundary layer becomes inverted at 4.8°C., the motion being upward when the bath temperature is less than 4.8°C. and downward when the bath temperature is greater. Upon this hypothesis, Merk (*6*) developed a theoretical expression relating the heat transfer coefficient for the physical properties of the fluid and the temperature difference which is in good agreement with the heat transfer coefficients measured by Dumore, Prins, and Merk. However, as has been pointed out, there is reason to suspect the formation of a dual motion rather than a simple inversion of the direction of motion.

QUALITATIVE OBSERVATIONS

An insight into the mechanism of natural convection in the region of maximum fluid density may be achieved by studying the fluid velocities within the boundary layers.

The velocities which are produced by density gradients in water, as measured by a visual technique, are about 1 cm./sec. Polystyrene particles (325–400 mesh) were introduced into the bath, and a beam of light was directed toward the plate. Light was reflected from the suspended particles and visually detectable by a lens system arranged as shown in Figure 2. A particle in motion could be observed and its speed determined by use of a stop watch and the increments of distance were furnished by an imposed grid system.

To test the accuracy of this technique of velocity measurement, three runs were performed in which the bulk temperature was fixed at such a level as to avoid maximum density within the boundary layer. The velocity distribution for this case has been computed numerically by Ostrach (*7*) using a digital computer and by Schechter (*10*) on an analogue computer. The experimental velocities are compared with the numerical solution obtained by Schechter and the results are shown in Figure 3. The experimental values of the velocity are consistently less than those predicted by the numerical solutions, the discrepancies probably being accounted for by the slightly greater particle density (1.05). The velocity measurements are within an accuracy of $\pm 25\%$.

For those runs in which the bath temperature was maintained below 4°C. the velocity pattern behaved qualitatively as follows.

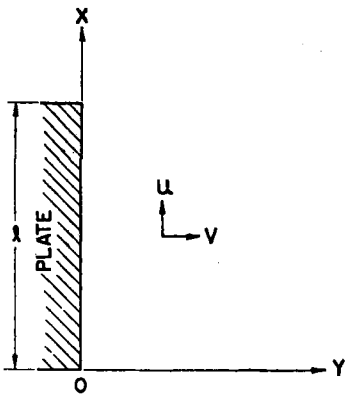

Fig. 1. Coordinate system for vertical plate.

1. As the plate is heated initially, the flow in the boundary layer is downward.
2. Increasing the plate temperature results in a decrease in the magnitude of the velocities.
3. If the plate temperature is increased sufficiently, a point of stagnation occurs near the plate surface; consequently, not only is the velocity at the surface of the plate zero, but the velocity gradient is also zero. It is under these conditions that the positive driving force near the surface offsets the negative force resulting from the viscous effects of the downward motion.
4. Any further increase in the plate temperature will result in a dual motion. The fluid near the plate will move upward and that in the outer portion of the boundary layer will move downward. A typical example of this dual motion is shown in Figure 4.

Those conditions which produce dual convection currents are termed *inverted convection regimes* and the cases in which only a falling or a rising film occur are called *normal*, or *unidirectional, convection regimes*.

A qualitative sketch of the velocity pattern existing at the upper edge of the plate is shown in Figure 5. In the inverted regime the portion of the fluid which is heated to a sufficiently high temperature will rise until it passes the upper edge of the plate. In the region above the heated plate the hot fluid will mix with the unheated fluid. When this interchange of heat has reduced the temperature level enough to yield a mixture having a density greater than that of the bulk fluid, the positive motion will be arrested and reversal of direction will occur. The result of this series of events is to produce a tendency for all the sensible heat being carried past the upper edge of the plate by the upward motion to return to the boundary layer in the form of sensible heat in the falling film. (This is true at least when a starting section is employed.) At the lower edge of the plate the situation is entirely different. Again the warm fluid mixes with the unheated fluid; however, the driving force remains negative and thus the heat continues to be carried downward.

THEORETICAL CONSIDERATIONS

The character of the heat transfer mechanism differs between the unidirectional and inverted convection regimes, and therefore each case will be considered separately.

Unidirectional Convection Regime

Approximate Solution: For many liquids the variation of the specific volume with temperature is reported in the literature in the form of a polynomial, such as

$$\frac{1}{\rho} = \frac{1}{\rho_0}(1 + A_1T + A_2T^2 + A_3T^3) \qquad (5)$$

Utilizing Equation (5), Merk (*6*) derived the buoyant force per unit mass as

$$g\left(\frac{\rho_\infty - \rho}{\rho}\right) = g\beta_\infty\theta_s(\phi + s_1\phi^2 + s_2\phi^3) \qquad (6)$$

Substituting Equation (6) for the driving-force term in Equation (1) yields

$$u\frac{\partial u}{\partial x} + v\frac{\partial u}{\partial y} = g\beta_\infty\theta_s(\phi + s_1\phi^2 + s_2\phi^3) + \nu\frac{\partial^2 u}{\partial y^2} \qquad (7)$$

If β_∞ is negative, the convection currents are always downward for a heating process, provided that dual convection currents do not exist. Consequently, it is convenient to translate the origin of the coordinate system to the upper edge of the plate.

Thus

$$w = 1 - x \qquad (8)$$

and

$$p = -u$$

Use of Equation (8) in Equations (7), (2), and (3) leads to the following set of equations for the downward convective current, which includes the density-temperature dependency:

$$p\frac{\partial p}{\partial w} + v\frac{\partial p}{\partial y} = \nu\frac{\partial^2 p}{\partial y^2} + g\gamma_\infty\theta_s(\phi + s_1\phi^2 + s_2\phi^3) \qquad (9)$$

$$\frac{\partial p}{\partial w} + \frac{\partial v}{\partial y} = 0 \qquad (10)$$

$$p\frac{\partial \phi}{\partial w} + v\frac{\partial \phi}{\partial y} = \alpha\frac{\partial^2 \phi}{\partial y^2} \qquad (11)$$

The boundary conditions are

$$p = 0 \quad \phi = 1 \quad \text{at} \quad y = 0$$
$$p = 0 \quad \phi = 0 \quad \text{at} \quad y = \infty \qquad (12)$$

The layers in which the velocity and the temperature differ significantly from the bulk conditions are thin. Each thickness has been termed the *boundary-layer* thickness and is denoted by the symbol δ. The thermal boundary layer is not, except in rare instances, equal to the hydrodynamic boundary layer; however for the purposes of this paper equal thicknesses have been assumed.

The velocity and temperature profiles are assumed to be expressible in the form of polynomials (*2*), which are

$$p = p_1\frac{y}{\delta}\left(1 - \frac{y}{\delta}\right)^2 \qquad (13)$$

and

$$\phi = \left(1 - \frac{y}{\delta}\right)^2 \qquad (14)$$

Integrating Equations (1) and (11) from 0 to δ with the aid of Equation (10) and substituting Equations (13) and (14) produces Equations (15) and (16):

$$\frac{d}{dw}\left(\frac{p_1^2\delta}{105}\right) = \delta\left[g\gamma_\infty\theta_s\left(\frac{1}{3} + \frac{s_1}{5} + \frac{s_2}{7}\right)\right] - \nu\frac{p_1}{\delta} \qquad (15)$$

and

$$\frac{d}{dw}\left(\frac{p_1\delta}{30}\right) = \frac{2\alpha}{\delta} \qquad (16)$$

Solving Equations (14) and (15) for δ and noting that $h_w = -2k/\delta$ yields the point Nusselt number:

$$Nu_w' = 0.669\,Pr^{1/2}(0.952 + Pr)^{-1/4}\cdot\left[Gr_w'\left(\frac{1}{3} + \frac{s_1}{5} + \frac{s_2}{7}\right)\right]^{1/4} \qquad (17)$$

The point heat transfer coefficient h_w is inversely proportional to the fourth root of w. By integration over the length of the plate, the average heat transfer coefficient is obtained:

$$\bar{h} = 4/3h_w \qquad (18)$$

The average Nusselt number is obtained by introducing Equation (18) into Equation (17) and eliminating h_w:

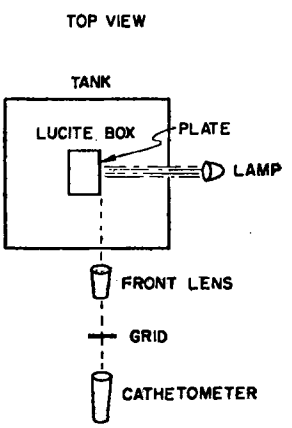

Fig. 2. Lighting system for velocity measurements.

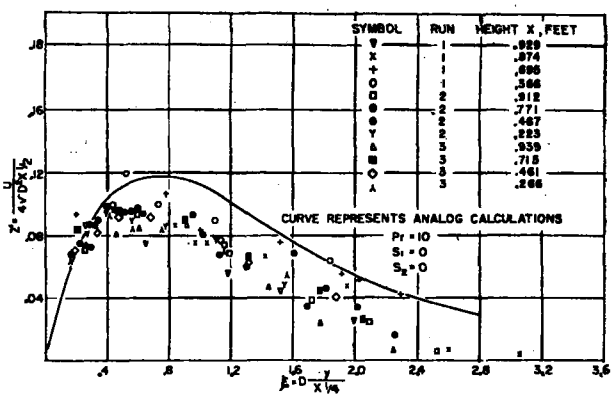

Fig. 3. Comparison of experimental and theoretical velocity distributions.

$$\overline{Nu} = 0.892\left[\overline{Gr}'\left(\frac{1}{3} + \frac{s_1}{5} + \frac{s_2}{7}\right)\right]^{1/4} \cdot Pr^{1/2}(0.952 + Pr)^{-1/4} \quad (19)$$

Equations (17) *and* (19) *have no physical* significance if $[(1/3) + (s_1/5) + (s_2/7)]$ *is less than, equal to, or approaches zero.* A negative value of the quantity $[(1/3) + (s_1/5) + (s_2/7)]$ leads to a negative Nusselt number if either Equation (17) or (19) is employed. If $[(1/3) + (s_1/5) + (s_2/7)]$ equals zero, then Equations (17) and (19) indicate that the Nusselt number should be zero. This result, however, is not correct. The minimum value of the Nusselt number corresponds to that of a purely conductive process.

The results of analogue solutions (presented in the following sestion) indicate that a condition of stagnation prevails at the surface of the plate $[(\partial p/\partial y) = 0$ at $y = 0]$ when $[(1/3) + (s_1/5) + (s_2/7)]$ equals zero. Consequently, the sign of the quantity $[(1/3) + (s_1/5) + (s_2/7)]$ is a criterion for determining the type of convection currents which may be expected. A positive value indicates that the convection currents are normal; a negative sign points to an inverted flow regime.

Analogue Computer Solution: Equations (17) and (19) are derived from several assumptions. It is useful to verify these equations by a more exact method.

A stream function is defined as follows:

$$\frac{\partial \Psi}{\partial y} = p \quad \text{and} \quad \frac{\partial \Psi}{\partial w} = -v \quad (20)$$

Substituting the stream function into Equations (10) and (11) yields

$$\frac{\partial \Psi}{\partial y}\frac{\partial^2 \Psi}{\partial w \partial y} - \frac{\partial \Psi}{\partial w}\frac{\partial^2 \Psi}{\partial y^2} = \nu \frac{\partial^3 \Psi}{\partial y^3} + g\gamma_\infty \theta_s(\phi + s_1\phi^2 + s_2\phi^3) \quad (21)$$

$$\frac{\partial \Psi}{\partial y}\frac{\partial \phi}{\partial w} - \frac{\partial \Psi}{\partial w}\frac{\partial \Psi}{\partial y} = \alpha \frac{\partial^2 \phi}{\partial y^2} \quad (22)$$

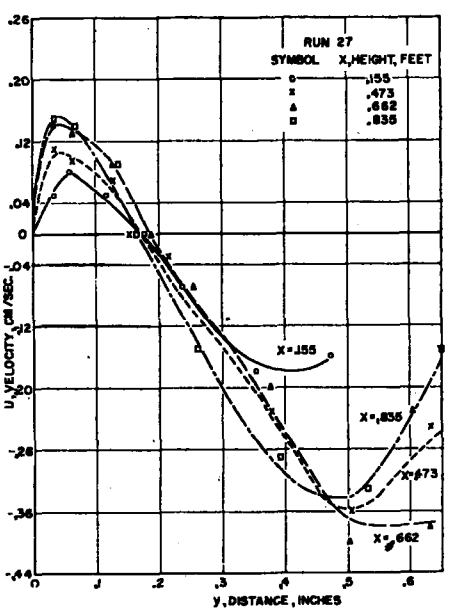

Fig. 4. Typical velocity distributions in inverted regime.

The boundary conditions are

$$\frac{\partial \Psi}{\partial y} = 0\ \frac{\partial \Psi}{\partial w} = 0\ \phi = 1 \text{ at } y = 0$$
$$\frac{\partial \Psi}{\partial y} = 0\ \frac{\partial \Psi}{\partial w} = 0\ \phi = 0 \text{ at } y = \infty \quad (23)$$

In order to reduce this system of partial differential equations to a system of ordinary differential equations, Pohlhausen's (*8*) substitutions are used. They are

$$\xi = \frac{cy}{w^{1/4}} \quad (24)$$

where

$$c = \sqrt[4]{\frac{g\gamma_\infty \theta_s}{4\nu^2}} \quad (25)$$

and

$$\eta(\xi) = \phi(w, y) \quad (26)$$

$$z(\xi) = \frac{\Psi(w, y)}{4\nu c w^{1/4}} \quad (27)$$

Substituting Equations (24), (26), and (27) into Equations (21) and (22) yields the following system of ordinary differential equations:

$$z''' + 3zz'' - 2(z')^2 + \eta + s_1\eta^2 + s_2\eta^3 = 0 \quad (28)$$

$$\eta'' + 3P_r\eta' = 0 \quad (29)$$

with boundary conditions

$$z = 0\ z' = 0\ \eta = 1 \text{ at } \xi = 0$$
$$z' = 0\ z'' = 0\ \eta = 0 \text{ at } \xi = \infty \quad (30)$$

Numerical solutions for this system of equations would be extremely difficult to obtain without the aid of a computing machine. A Reeves Electronic Analogue Computer was used to solve the set of Equations (28), (29), and (30). A schematic diagram of the wiring circuit is shown in Figure 6. The symbols used are those suggested by Korn and Korn (*5*).

The technique of trial and error is involved in obtaining the analogue solutions, because all the initial conditions (initial conditions refer to the values of the functions and their derivatives at $\xi = 0$) must be known in order to start the solution on the computer; hence, values of z'' and η' at $\xi = 0$ were assumed and if the boundary conditions at $\xi = \infty$ were fulfilled, the assumed initial values are correct.

A series of analogue solutions was obtained for a value of the Prandtl number equal to 10 (approximately that of water). Each solution is termed a *result.* The values of the two parameters, s_1 and s_2, were chosen so that result I corresponds to the situation in which the bulk temperature is 0°C. and the plate temperature is 1°C. By the same token, result II corresponds to a plate temperature at 2°C. and a bulk temperature of

0°C. Solutions were obtained for 1°C. increments of plate temperature up to and including a plate temperature of 14°C. the bulk temperature being held constant at 0°C.

The value of z'' at $\xi = 0$ is zero when the plate temperature is 14°C. (result XIV). This is the transition point. Any further increase in the plate temperature would result in inverted convection currents. *In the inverted-convection regime, Pohlhausen's substitutions are no longer valid because they require that the velocities and temperatures at $y = \infty$ equal the velocities and temperatures at $w = 0$* ($\xi = \infty$ at both $y = \infty$ and at $w = 0$). This limits the application of Equations (28), (29), and (30) to normal convective regimes.

It is of interest to note that for a bulk temperature of 0°C. the value of $[(1/3) + (s_1/5) + (s_2/7)]$ is zero at a plate temperature of 13.60°C., a value which is in excellent agreement with the value of 14°C. obtained as the transition point from the more exact analogue solutions.

Figures 7 and 8 show the velocity and temperature patterns as the plate temperature is increased. As the plate temperature is increased (increasing result numbers), the initial slope of the velocity and temperature curves decreases. The initial temperature gradient varies from -1.185 at $s_1 = s_2 = 0$ to -0.882 at the transition point, a change of 34%. This illustrates the necessity of considering parameters s_1 and s_2 when natural-convection heat transfer coefficients are computed in a region of maximum density. A summary of all analogue solutions is presented in Table 1.

A comparison of the approximate analytical solution, Equation (19), and the analogue solutions is shown in Table 2. The average Nusselt number can be computed from the analogue data by applying the following relationship:

$$\overline{Nu} = -0.943(\overline{Gr}')^{1/4}\left(\frac{d\eta}{d\xi}\right)_{\xi=0} \qquad (31)$$

The approximate solution yields results which are low near the transition point. The average Nusselt number calculated from Equation (19) is 14% less than the value indicated by the analogue solution when $[(1/3) + (s_1/5) + (s_2/7)]$ equals $+0.064$. The disagreement becomes more pronounced as the value of $[(1/3) + (s_1/5) + (s_2/7)]$ approaches zero.

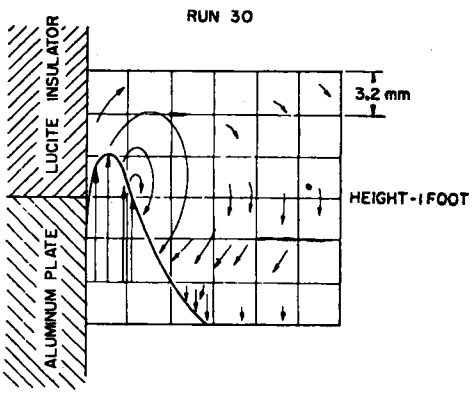

Fig. 5. Flow patterns at top of plate for inverted regime.

Inverted Convection Regime

Conditions for Model: All the sensible heat in the rising fluid which passes the upper edge of the plate will be assumed to return to the boundary layer in the form of sensible heat in the falling layer. This can be expressed as follows:

$$\left(\int_0^\delta u\phi\, dy\right)_{x=l} = 0 \qquad (32)$$

As a corollary, all heat transferred from the plate must pass the lower edge of the plate in the form of sensible heat of the falling film. This can be expressed as follows:

$$\left(\int_0^\delta u\phi\, dy\right)_{x=0} = -\frac{\bar{h}l}{C_p\rho} \qquad (33)$$

The velocity profile which was assumed in deriving the approximate solution for the case of normal convection [Equation (13)] must be altered to conform to the pattern of dual motion. Since there is both a positive and a negative flow, the velocity, u, will be equal to zero at some point within the boundary layer. This may be called point of zero velocity, δ_i. A polynomial of fourth order is assumed which satisfies both the boundary conditions plus a smooth-fit condition [$(du/dy) = 0$ at $y = \delta$] and a zero at $\delta_i (u = 0$ at $y = \delta_i)$. This polynomial is

$$u = \frac{E(x)}{2}\left\{\left[\left(\frac{y}{\delta}\right) - 3\left(\frac{y}{\delta}\right)^3 + 2\left(\frac{y}{\delta}\right)^4\right] - G\left[\left(\frac{y}{\delta}\right) - 2\left(\frac{y}{\delta}\right)^2 + \left(\frac{y}{\delta}\right)^3\right]\right\} \qquad (34)$$

The introduction of the new variable δ_i yields a system of two equations and three unknowns. In order to render this system solvable, a net vertical downward flow will be postulated such that

$$\int_0^\delta u\, dy = C_0 \qquad (35)$$

Equation (35) implies that none of the fluid medium enters or leaves the boundary layer except at the top or the bottom of the plate.

Equation (14) will be taken to be valid in the inverted regime as well as for normal convection.

Approximate Solution: If Equation (6) is substituted into Equation (1) and the resulting expression integrated from 0 to δ (it being assumed that the hydrodynamic-boundary-layer thickness equals the thickness of the thermal boundary layer), one obtains with the aid of Equation (2)

$$\frac{d}{dx}\int_0^\delta u^2\, dy = \int_0^\delta g\beta_\infty\theta_s(\phi + s_1\phi^2 + s_2\phi^3)\, dy - \nu\left(\frac{\partial u}{\partial y}\right)_{y=0} \qquad (36)$$

Similarly if Equation (3) is integrated between the same limits with the aid of Equation (2), one gets

$$\frac{d}{dx}\int_0^\delta u\phi\, dy = -\alpha\left(\frac{d\phi}{dy}\right)_{y=0} \qquad (37)$$

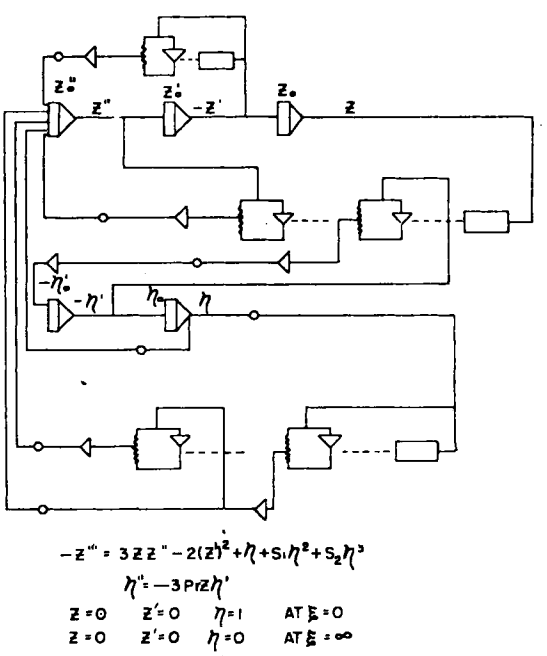

Fig. 6. Analogue-computer circuit and equations used in numerical solutions.

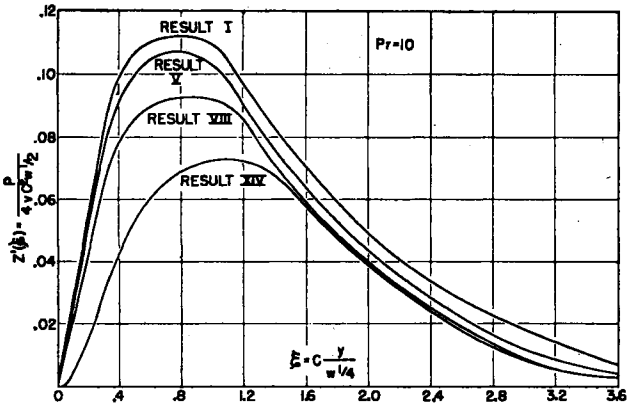

Fig. 7. Theoretical solutions obtained from analogue computer.

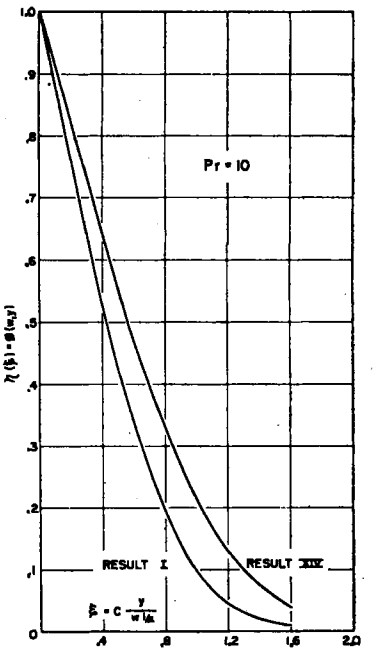

Fig. 8. Theoretical solutions obtained from analogue computer.

If the inertia term is neglected [left-hand side of Equation (36)], the system of Equations (14), (32), (33), (34), (36), and (37) can be handled in much the same manner as in the Squire-Eckert approach. The final equations for the point and average Nusselt numbers are the following:

$$Nu_x = 0.489\left[Gr_x Pr\left(\frac{1}{3}+\frac{s_1}{5}+\frac{s_2}{7}\right)\right]^{1/4} \quad (38)$$

$$\overline{Nu} = 0.652\left[\overline{Gr}Pr\left(\frac{1}{3}+\frac{s_1}{5}+\frac{s_2}{7}\right)\right]^{1/4} \quad (39)$$

[Other forms of Equations (38) and (39) have been obtained (*10*) by use of a model in which the condition given by Equation (33) has been replaced.]

The experimental observations indicate a finite boundary layer at $x = 0$; however, Equation (38) predicts an infinite point heat transfer coefficient, or zero boundary-layer thickness. The sensible-heat flow is accounted for in the following manner. The substitution of the polynomials relating ϕ and u to δ [Equations (14) and (34)] into Equation (33) and the integration lead to

$$(E\delta)_{x=0} = 105\,\frac{\bar{h}l}{\rho C_p} \quad (40)$$

Equation (40) indicates that, even though the boundary-layer thickness is extremely small, the velocity is so large at this point that the requisite quantity of heat leaves the boundary layer.

EXPERIMENTAL

A 1-ft.-square vertical heated plate was mounted within a large insulated tank containing water. The inside dimensions of the tank are 26 in. in length by 36 in. in width, by 36 in. in depth. To retain conditions of interest, it was necessary to maintain the bulk temperature of the water below 4°C.; consequently, the entire apparatus was installed in a constant-temperature room which enabled the experiments to be conducted in an ambient temperature approximately equal to that of bulk-water temperature.

Vertical temperature gradients within the tank were minimized through the use of a copper-coil cooling system positioned vertically along the walls of the tank. The coolant, a solution of ethylene glycol and water, was pumped through the coils from a refrigerated constant-temperature bath.

The heated test section was made from a 12- by 12- by ¾-in. aluminum plate. Grooves were milled into the back of the plate and into these grooves were fitted porcelain insulators containing No. 20 B. & S. gauge nichrome IV wire. The insulators were fixed into place with sauereisen electrical cement. Four parallel heater circuits were used, each independently controlled. The wires were spaced so that each carried an equal heat load when the convection currents were normal. A detailed analysis of the required spacing was done by Weingarden (*12*). Figure 9 shows the spacing and also the wiring of the four heater sections. These sections are designated I, II, III, and IV as shown in the sketch. The numbered circles represent the positions of the ten 20-gauge copper-constantan thermocouples which were mounted into the back of the plate to within $\frac{1}{16}$ in. of the heat transfer surface.

As shown in Figure 10, the plate was mounted onto a Lucite box, which was filled with vermiculite to minimize heat losses. The box was positioned in the tank by vertical bar mounts.

The power supply consisted of four 6-volt storage batteries and a rectifier, placed in parallel. The voltage of the rectifier was adjusted so that only a slight current was

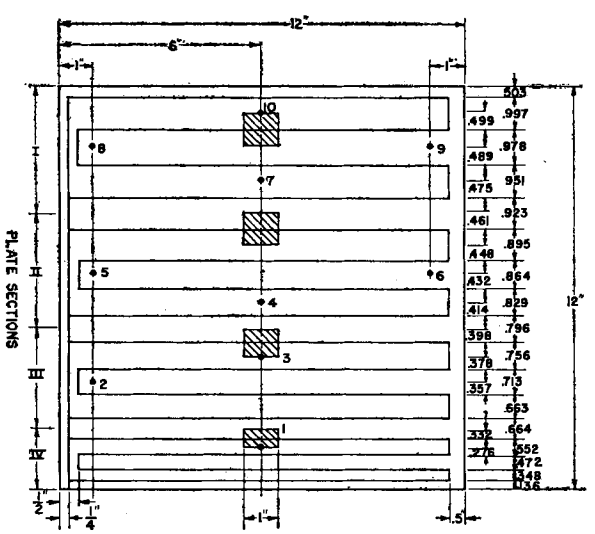

Fig. 9. Location of heater coils and thermocouples in test section.

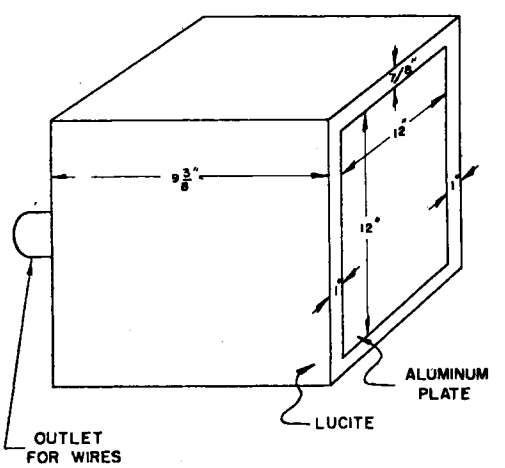

Fig. 10. Mounting of test plate in Lucite box.

drawn from the batteries. This gave voltages with less than 1% drift over an 8-hr. period and reduced instantaneous fluctuations. During operation the voltage drops across the heater circuits and calibrated manganin resisters were measured. From this information the power input could be calculated.

A temperature probe was constructed for the purpose of obtaining point coefficients. The probe consisted of a brass tube with a fork attachment at one end as shown in Figure 11. Across the tips of the fork was soldered a thermistor, which served as a resistance thermometer. This device was mounted into a slider. A vernier caliper was fixed on the slider so that changes of position might be measured with an accuracy of ±0.003 in. The thermistor used is a glass-coated bead 0.015 in. in diameter with 0.001-in. platinum lead wires extending from each end.

Figure 12 shows the complete electrical wiring of the apparatus.

The thermocouples and the thermistor were calibrated in the assembled apparatus. Beckman thermometers, set at the ice point, served as secondary standards. The estimated accuracy of the calibration was 0.01°C.

TEST RUNS

A total of twenty runs was made in which the flow in the boundary layer was unidirectional. The fluid film was rising during runs 1, 2, and 3 (the bulk temperature of the water being greater than 4°C.), and during runs 4 through 20 the film was falling. Runs 21 through 30 deal with the inverted-flow regime. In order to reduce the temperature gradients within the bath, ice was introduced into the bath before runs 4 to 10, 13 to 18, and 21 to 25 were made. (Ice was not introduced during the other runs in order to obtain data with higher bulk temperatures.) in all runs the water level was maintained at least 10 in. above the upper edge of the plate. Despite all precautions a temperature gradient still persisted during all the runs. The maximum vertical gradient was approximately 0.30°C./ft. with ice present within the tank. Without ice in the tank, the maximum temperature gradient was about 1.6°C./ft., and the mean gradient was 0.65°C./ft. Heat losses were neglected in the evaluation of heat transfer coefficients. For nearly all runs the maximum estimated heat loss ranged from 2 to 4.3% of the total heat input.

The viscosity was evaluated at the wall temperature as suggested by Schmidt and Beckmann (*11*). All other fluid properties were evaluated at the arithmetic mean of the wall and bulk temperatures.

DISCUSSION OF RESULTS

Standard Runs

The data for the initial three runs are given in Table 3. These runs were conducted with the bulk-water temperature maintained at a level to avoid the region of maximum density (i.e., $T_\infty > 4$°C.). The results of the experimental Nusselt numbers are shown together with the theoretical value [computed from Equation (19) with $s_1 = s_2 = 0$]. The maximum deviation of the experimental Nusselt number from the theoretical value is 7%. The experimental values are lower than the theoretical values, which may in part be attributed to the starting sections used along the upper and lower edges of the plate. These sections would tend to yield a thicker boundary layer and hence a smaller heat transfer coefficient. In the computation of the Grashof number for these three runs, the coefficient of expansion was calculated by the method suggested by Saunders (*9*),

$$\beta_f = \frac{\rho_\infty - \rho_f}{\rho_f(T_f - T_\infty)}$$

The coefficient of expansion for all other runs was calculated by employing either β_∞ or γ_∞.

Unidirectional convection: A comparison of the experimental average Nusselt numbers for falling films with the values obtained from Equation (19) is presented in Figure 13, with the exception of one experiment, the percentage deviation of the experimental values of the Nusselt number from the theoretical values is less than 13%, with a mean deviation of 4.7%. The largest deviations occur when the value of $[(1/3) + (s_1/5) + (s_2/7)]$ becomes small (i.e., less than 0.1). These deviations are to be expected, for as noted under Theoretical Considerations, the Nusselt number approaches a minimum value rather than zero.

Inverted Convection: The comparison of the predicted Nusselt number for the inverted regime with the experimental is shown in Figure 14. Except for runs 24 and 25, which are 15.6 and 42% in error, respectively, the maximum deviation for all runs in the inverted regime was less than 10% and the mean deviation was 3.3%. The theoretical value of the Nusselt number is expected to be smaller than the experimental value as the absolute value of the quantity $[(1/3) + (s_1/5) + (s_2/7)]$ approaches zero. Run 25 represents conditions in which the absolute value of $[(1/3) + (s_1/5) + (s_2/7)]$ is exceedingly small (0.00577), and hence the 42% deviation is not surprising. As noted previously, the model used for the theoretical equation does not provide for the conduction of heat through the stagnant film.

Velocity and Temperature Distributions: Figures 3, 14, 15, and 16 compare the results of the velocity and temperature measurements with those obtained from the solutions on the analogue computer. The agreement appears to be quite good for the case of the temperature profiles. Although the velocity data deviate somewhat from the predicted values, the authors believe that these deviations are due to the experimental difficulties en-

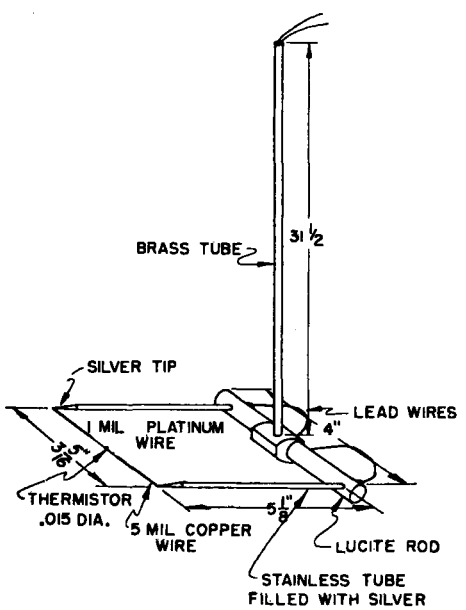

Fig. 11. Temperature probe.

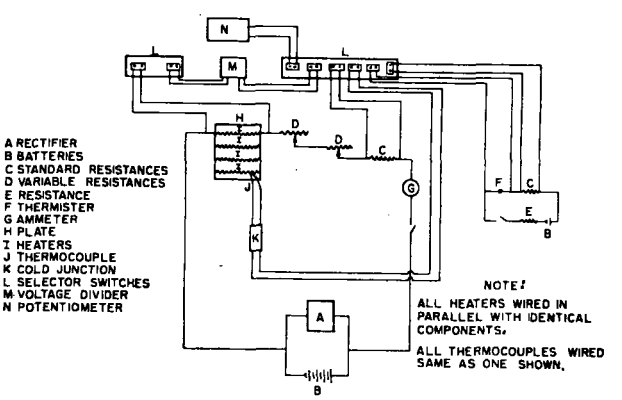

Fig. 12. Electrical circuit.

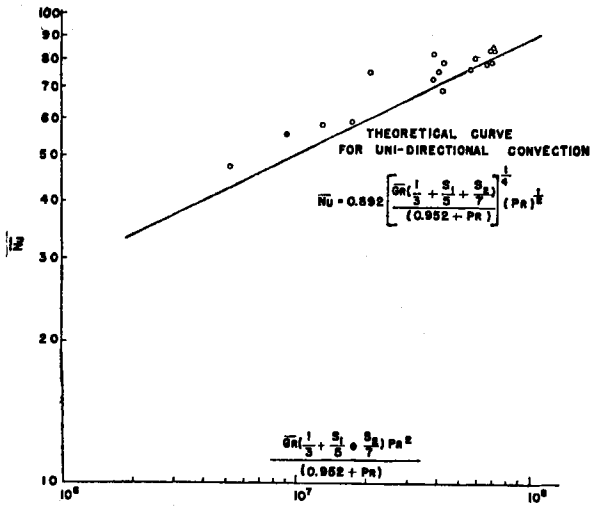

Fig. 13. Comparison of theoretical and experimental results for unidirectional convection.

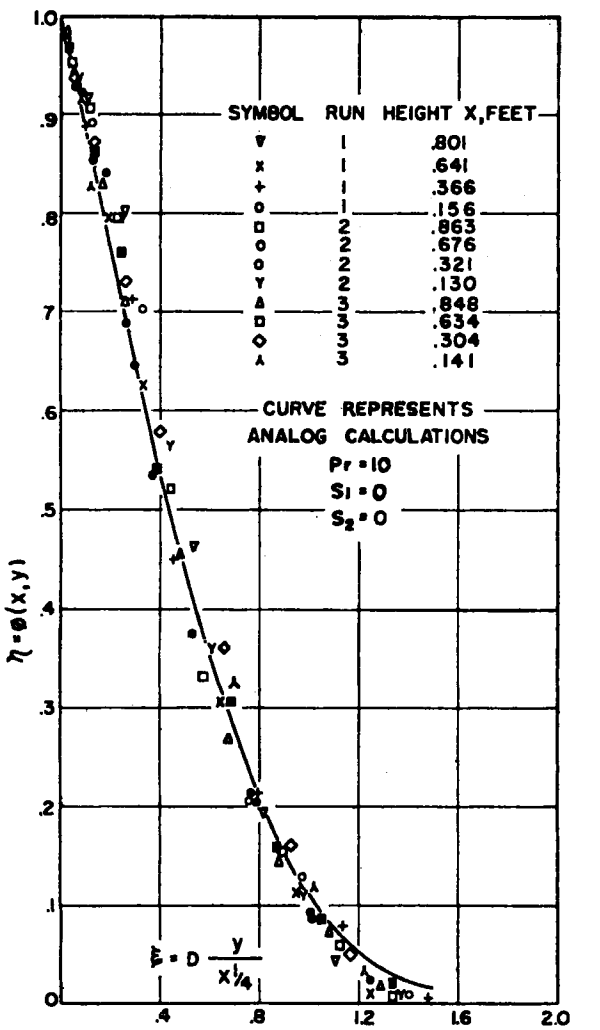

Fig. 15. Comparison of experimental and numerical temperature distributions.

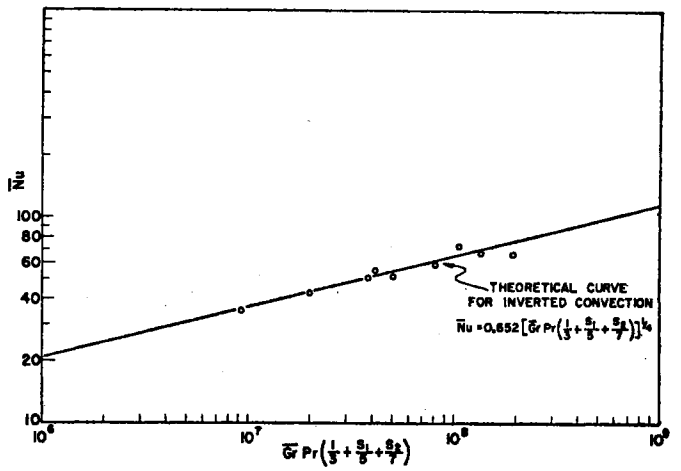

Fig. 14. Comparison of experimental and theoretical results, inverted regime.

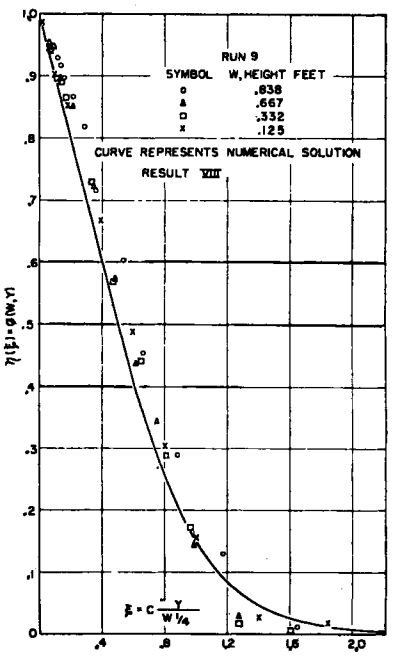

Fig. 16. Comparison of experimental and theoretical temperature distributions.

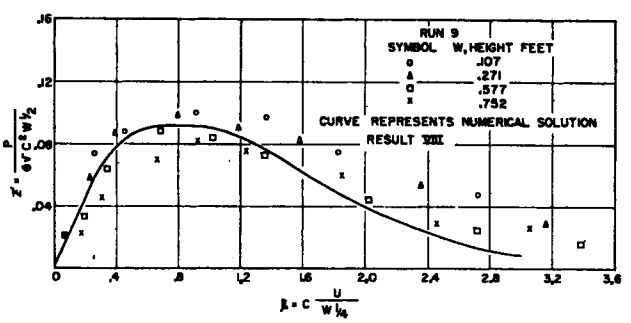

Fig. 17. Comparison of experimental and theoretical temperature distributions.

countered in attempting accurately to measure velocities of the magnitude encountered in natural convection.

The results presented in Figures 3 and 15 are those obtained from the standard runs. The data shown in Figures 16 and 17 are representative of all data taken in the unidirectional regime.

Two techniques of ascertaining the validity of the constant-net-flow assumption were tried; however, the experimental difficulties masked the comparisons. The velocity profiles at several positions along the plate were integrated and a deviation of $\pm 25\%$ from the constant-flow assumption was found. The point of zero velocity, δ_i, was measured for several runs and compared with the value for δ_i, solved from Equations (32), (34), (35), (36), and (37). The theoretical values for δ_i ranged from one-third to almost twice the experimental values. (Out of fourteen comparisons, only two theoretical values exceeded the experimental values.) One

TABLE 1

ANALOGUE RESULTS

Unidirectional Convection Regime

Result*	Parameters P_r	S_1	S_2	Analogue computer results $\left(\frac{d\eta}{d\xi}\right)_{\xi=0}$	$\left(\frac{d^2Z}{d\xi^2}\right)_{\xi=0}$
0	10	0	0	−1.185	0.440
I	10	−0.132	0.00106	−1.173	0.415
II	10	−0.264	0.00420	−1.157	0.390
III	10	−0.396	0.00945	−1.146	0.380
IV	10	−0.528	0.0168	−1.134	0.360
V	10	−0.660	0.0263	−1.118	0.340
VI	10	−0.792	0.0378	−1.091	0.310
VII	10	−0.924	0.0515	−1.073	0.290
VIII	10	−1.056	0.0672	−1.041	0.260
X	10	−1.320	0.105	−1.025	0.240
XI	10	−1.452	0.127	−0.972	0.165
XII	10	−1.584	0.151	−0.959	0.140
XIII	10	−1.716	0.178	−0.921	0.110
XIV	10	−1.848	0.206	−0.882	0
For Result 0, the following values have been reported (7):				−1.169	0.4192

*Bulk water temperature, 0°C.; plate temperature corresponds to result number in °C.

TABLE 2

COMPARISON OF ANALOGUE AND APPROXIMATE SOLUTIONS

Unidirectional Convection Regime

Pr	s_1	s_2	Approximate [Equation (19)] $\frac{\overline{Nu}}{(\overline{Gr}')^{1/4}}$	Analogue Results $\frac{\overline{Nu}}{(\overline{Gr}')^{1/4}}$	$\frac{1}{3}+\frac{s_1}{5}+\frac{s_2}{7}$
10	0	0	1.176	1.117	0.333
10	−0.132	0.00105	1.154	1.106	0.307
10	−0.266	0.00420	1.129	1.091	0.281
10	−0.396	0.00945	1.103	1.081	0.255
10	−0.528	0.0168	1.074	1.069	0.230
10	−0.660	0.0263	1.044	1.054	0.205
10	−0.792	0.0378	1.010	1.029	0.180
10	−0.924	0.0515	0.974	1.012	0.155
10	−1.056	0.0672	0.934	0.982	0.131
10	−1.320	0.105	0.836	0.967	0.084
10	−1.452	0.127	0.771	0.917	0.061
10	−1.584	0.151	0.685	0.904	0.036
10	−1.716	0.178	0.546	0.868	0.015
10	−1.848	0.206	0	0.832	−0.007

TABLE 3

STANDARD RUNS*

Comparisons of Experimental and Theoretical Results

Run	T_p, °C.	T_∞, °C.	$\frac{1}{3}+\frac{s_1}{5}+\frac{s_2}{7}$	$\overline{Gr} \times 10^{-7}$	Pr	$\overline{Nu}$ theoretical†	$\overline{Nu}$ experimental
1	13.36	9.24	0.333	6.992	8.59	103.4	96.9
2	11.71	8.84	0.333	4.189	8.98	92.1	86.1
3	9.83	7.78	0.333	2.124	9.52	78.9	75.5

*The unidirectional heat transfer tests for runs 1, 2, and 3 represent critical evaluations of the experimental procedures and therefore are termed *standard* runs.

†Equation (19): $\overline{Nu} = 0.892\left[\overline{Gr}'\left(\frac{1}{3}+\frac{s_1}{5}+\frac{s_2}{7}\right)\right]^{1/4} Pr^{1/2}(0.952+Pr)^{-1/4}$.

For $\left(\frac{1}{3}+\frac{s_1}{5}+\frac{s_2}{7}\right) = 0.333$, Equation (19) reduces to Eckert's theoretical equation.

$Nu = 0.68\left(\frac{Pr}{0.952+Pr}\right)^{1/4}(Pr\,\overline{Gr}')^{1/4}$ (fluid properties evaluated at film temperature)

inaccuracy of the theoretical treatment is the assumption that the thermal boundary layer thickness equals that of the hydrodynamic boundary layer. Howrath (3) has demonstrated that this ratio should be of the order $(Pr)^{1/2}$.

The profiles presented in Figure 19 serve to support the assumption concerning the return of sensible heat to the boundary layer. If the product $u\phi$ is measured at several points and the resulting curve graphically integrated, 108% of the sensible heat contained in the rising portion of the boundary layer is found in the falling stream. The velocity measurements shown in Figure 19 were taken at $x = 0.833$ ft., and the temperature profile is for a height of 0.828 ft. from the lower edge of the plate. Thus if all the sensible heat passing the upper edge of the plate reenters the boundary layer, the falling film would be expected to contain an amount of heat equal to that of the rising film plus the quantity of heat convected to the falling stream in the upper 0.172 ft. of the plate.

Point heat transfer coefficients were calculated by extrapolating the temperature profile to $y = 0$ and determining the temperature gradient at the wall. As this method did not yield consistent results, it is not reported here.

CONCLUSIONS

Convective heat transfer is greatly influenced by the presence of a density maximum in the convecting fluid, which leads to two convective mechanisms, each of which must be considered separately. These two convective regimes have been termed *normal*, or *unidirectional*, convection and *inverted* convection. A test was devised to predict the type of regime that will prevail for given conditions of plate and bulk temperature. This test may be stated as follows:

If

$$\frac{1}{3}+\frac{s_1}{5}+\frac{s_2}{7} < 0$$

inverted convection

$$\frac{1}{3}+\frac{s_1}{5}+\frac{s_2}{7} \geq 0$$

normal convection

Heat transfer coefficients can be predicted for both regions with a deviation in the Nusselt number of ±10%, provided that $[\frac{1}{3} + (s_1/5) + (s_2/7)] > 0.05$, by use of Equation (19) or (39), depending on the convective regime.

ACKNOWLEDGMENT

The research was supported by a grant from the National Science Foundation to the Department of Chemical Engineering. A fellowship from the Allied Chemical and Dye Corporation is also gratefully acknowledged.

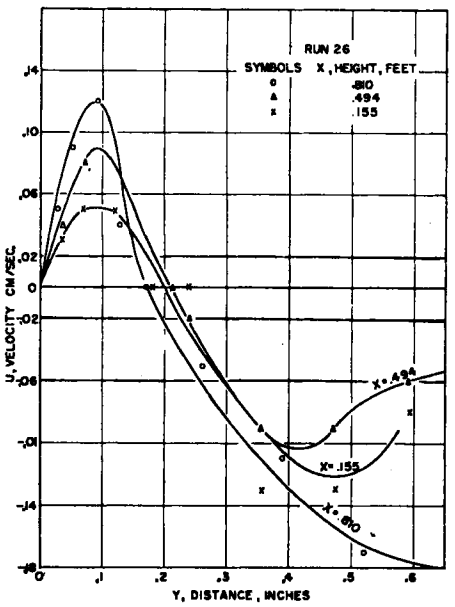

Fig. 18. Comparison of experimental and theoretical velocity distributions.

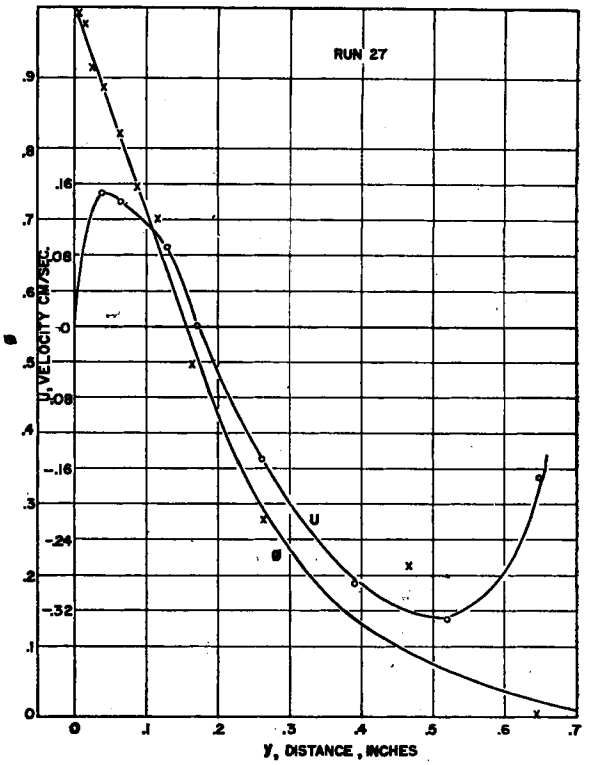

Fig. 19. Typical velocity distributions in inverted regime.

NOTATION

A_1, A_2, A_3 = constants in equation of state
C_p = heat capacity of fluid
$C = \sqrt[4]{\frac{g\gamma_\infty\theta_s}{4\nu^2}}$
$D = \sqrt[4]{\frac{g\beta_f\theta_s}{4\nu^2}}$
E = function of x
$G = 1 + 2\frac{\delta_i}{\delta}$
$Gr_w' = \frac{g\gamma_\infty\theta_s w^3}{\nu^2}$
$\overline{Gr}_w' = \frac{g\gamma_\infty\theta_s l^3}{\nu^2}$
$Gr_x = \frac{g\beta_\infty\theta_s x^3}{\nu^2}$
$\overline{Gr} = \frac{g\beta_\infty\theta_s l^3}{\nu^2}$
g = acceleration due to gravity
h_x, h_w = point heat transfer coefficients
$\bar{h}$ = over-all heat transfer coefficient
k = thermal conductivity of fluid
l = height of plate
$Nu_w = \frac{h_w w}{k}$
$Nu_x = \frac{h_x x}{k}$
$\overline{Nu} = \frac{\bar{h} l}{k}$
$N = 1 + A_1T_\infty + A_2T_\infty^2 + A_3T_\infty^3$
p = velocity, positive for downward motion
p_1 = function of w only
$Pr = \frac{C_p\mu}{k}$
$s_1 = \frac{(A_1 + 3A_2T_\infty)\theta_s}{N\beta_\infty}$
$s_2 = \frac{A_3\theta_s^2}{N\beta_\infty}$
T = temperature of fluid at a point
T_∞ = bulk temperature at fluid
T_p = surface temperature of plate
$T_f = \frac{T_p + T_\infty}{2}$
u = velocity in x direction, positive for upward motion
v = velocity in y direction
$w = 1 - x$
x = distance in vertical direction
y = distance in horizontal direction

Greek Letters

$\alpha = \frac{k}{C_p\rho}$
$\beta_\infty = \frac{A_1 + 2A_2T_\infty + 3A_3T_\infty^2}{N}$
$-\gamma_\infty = \beta_\infty$
δ = boundary layer thickness
δ_i = distance measured from plate to point of velocity inversion
$\theta_s = T_p - T_\infty$
μ = dynamic viscosity
ν = kinematic viscosity
ρ = density of fluid
ρ_∞ = density of fluid evaluated at T_∞
ρ_f = density of fluid evaluated at T_f
$\phi = \frac{T - T_\infty}{T_p - T_\infty}$
Ψ = stream function

LITERATURE CITED

1. Dumore, J. M., H. J. Prins, J. A. Merk, *Nature*, **172**, 460 (1953).
2. Eckert, E. R. G., "Introduction to the Transfer of Heat and Mass" McGraw-Hill Book Company, Inc., New York (1950).
3. Howrath, Leslie, "Modern Developments in Fuid Dynamics," vol. 1, Oxford University Press, New York (1953).
4. Jakob, Max, "Heat Transfer," vol. 1, Wiley and Sons, Inc., New York (1950).
5. Korn, G. A., and T. M. Korn, "Electronic Analog Computers," McGraw-Hill Book Company, Inc., New York (1952).
6. Merk, H. J., *Appl. Sci. Research.* **4**, Sec. A, 435 (1953).
7. Ostrach, S., *Natl. Advisory Comm. Aeronaut. Tech. Note* 2635 (1952).
8. Pohlhausen, E., in Jakob, *op. cit.*
9. Saunders, O. A., *Proc. Roy. Soc.* (*London*), **A172**, 55 (1939).
10. Schechter, R. S., Ph.D. thesis, Univ. Minn., Minneapolis (1956).
11. Schmidt, E., and W. Beckmann, in Jakob, *op. cit.*
12. Weingarden, Morris J., M.S. thesis, Univ. Minn., Minneapolis (1955).

Manuscript received in editorial office Feb. 27, 1957; revision received Oct. 4, 1957; paper accepted Oct. 28, 1957.